1,25(OH)$_2$D$_3$ ameliorates doxorubicin-induced cardiomyopathy by inhibiting the NLRP3 inflammasome and oxidative stress

XIN GU[1*], LIN ZHAO[1*], JIABAO YE[2*], LIN CHEN[2], CHENYAN SUI[3], BAIHONG LI[1], XIAOYAN WANG[1], JUN ZHANG[2] and YINGQIANG DU[2]

[1]Department of Cardiology, The Affiliated Hospital of Jiangnan University, Wuxi, Jiangsu 214062;
[2]Department of Cardiology, The Affiliated Suzhou Hospital of Nanjing Medical University,
Suzhou Municipal Hospital, Gusu School, Nanjing Medical University, Suzhou, Jiangsu 215008;
[3]Department of Neurology, The Affiliated Hospital of Jiangnan University, Wuxi, Jiangsu 214062, P.R. China

Abstract. Doxorubicin (DOX), as a chemotherapy agent with marked therapeutic effect, can be used to treat certain types of cancer such as leukemia, lymphoma and breast cancer. However, the toxic effects of DOX on cardiomyocytes limit its clinical application. Oxidative stress has been documented to serve a pivotal role in DOX-induced cardiomyopathy. Previous studies have reported that 1,25(OH)$_2$D$_3$ has anti-oxidant and anti-inflammatory effects and can inhibit the renin-angiotensin system. However, the effects of 1,25(OH)$_2$D$_3$ on the pathophysiological processes of DOX-induced cardio-myopathy and its mechanisms remain poorly understood. To investigate these potential effects, C57BL/6J mice were used to construct a DOX-induced cardiomyopathy model and treated with 1,25(OH)$_2$D$_3$. At 4 weeks after the first injection of DOX, cardiac function and myocardial injury were evaluated by echocardiograph and ELISA. Masson's trichrome staining and RT-qPCR were used to assess myocardial fibrosis, and immunohistochemistry and western blotting were performed to analyze expression levels of inflammation and oxidative stress, and the NLRP3 inflammasome pathway. ChIP assay was used to assess the effects of 1,25(OH)$_2$D$_3$ on histone modification in the NLRP3 and Nrf2 promoters. The results showed that 1,25(OH)$_2$D$_3$ treatment increased LVEF and LVFS, reduced serum levels of BNP and cTnT, inhibited the collagen deposition and profibrotic molecular expression, and downregulated the levels of inflammatory cytokines in DOX-induced cardiomyopathy. ROS and antioxidant indices were also ameliorated after 1,25(OH)$_2$D$_3$ treatment. In addition, 1,25(OH)$_2$D$_3$ was found to inhibit the NLRP3 inflammasome and KEAP-Nrf2 pathways through regulation of the levels of H3K4me^3, H3K27me^3 and H2AK119Ub in the NLRP3 and Nrf2 promoters. In conclusion, the present study demonstrated that 1,25(OH)$_2$D$_3$ regulated histone modification in the NLRP3 and Nrf2 promoters, which in turn inhibits the activation of NLRP3 inflammasome and oxidative stress in cardiomyocytes, alleviating DOX-induced cardiomyopathy. Therefore, 1,25(OH)$_2$D$_3$ may be a potential drug candidate for the treatment of DOX-induced cardiomyopathy.

Introduction

As a classical antitumor drug, doxorubicin (DOX) serves a key role in chemotherapy against a number of tumor types such as leukemia, lymphoma and breast cancer (1,2). However, DOX treatment may also induce cardiomyopathy, which adversely affects patient outcome (3,4). DOX-induced cardiomyopathy causes severe cardiac dysfunction, which mainly manifests as a decrease in cardiac ejection fraction (5). DOX-induced cardio-myopathy is an acute complication of long-term chemotherapy and can lead to an increased mortality rate in patients (6). The pathogenesis of DOX-induced cardiomyopathy is complex and remains unclear. Due to the lack of specific therapeutic drugs, patients with DOX-induced cardiomyopathy can only been given symptomatic relief and supportive treatment (7). Therefore, it is necessary to explore the pathophysiological processes of DOX-induced cardiomyopathy and investigate potential efficacious approaches for treatment.

1,25(OH)$_2$D$_3$ is a metabolic derivative of vitamin D3 that is also a steroid hormone (8). 25-hydroxyvitamin D3 [25(OH)D$_3$] is the major circulating form of vitamin D. 25(OH)D$_3$ metabolizes to 1,25(OH)$_2$D$_3$ by catalysis of the renal 25(OH)D1α hydroxylase (CYP27B1) (9). 1,25(OH)$_2$D$_3$ serves an important role in regulating calcium homeostasis, bone metabolism and the immune system (10,11). Previous studies have reported that CYP27B1 is mainly expressed in

Correspondence to: Dr Yingqiang Du or Dr Jun Zhang, Department of Cardiology, The Affiliated Suzhou Hospital of Nanjing Medical University, Suzhou Municipal Hospital, Gusu School, Nanjing Medical University, 242 Guangji Road, Suzhou, Jiangsu 215008, P.R. China
E-mail: yingqiangdu@njmu.edu.cn
E-mail: zhangjun0808@njmu.edu.cn

*Contributed equally

the kidney, but an increasing number of studies have reported that CYP27B1 is widely expressed in multiple organs and various cell types, such as the lungs, intestines, skin, keratinocytes, macrophages and osteoblasts, indicating that the targets of 1,25(OH)$_2$D$_3$ are extensive and complex (12,13). Vitamin D has also been reported to exert protective effects against cardiovascular disease (14) and diabetic cardiomyopathy (15). Patients with dilated cardiomyopathy tend to have lower levels of 25-hydroxyvitamin D3 in the serum compared with those subjects without dilated cardiomyopathy (16). The mechanism by which vitamin D protects against cardiomyopathy is mainly attributed to its antioxidant, anti-inflammatory and inhibitory effects on the renin-angiotensin system (17,18). However, whether 1,25(OH)$_2$D$_3$ can protect against the pathophysiological processes of DOX-induced cardiomyopathy and its mechanisms remain unknown.

The nod-like receptor family pyrin domain containing 3 (NLRP3) inflammasome is a protein complex that recognizes a diverse array of extracellular and intracellular signals, including damage-associated molecular patterns and pathogen-associated molecular patterns (19). Activation of the NLRP3 inflammasome pathway induces production of proinflammatory cytokines, such as IL-1β and IL-18, to generate a proinflammatory microenvironment and inflammageing (20). However, the relationship between 1,25(OH)$_2$D$_3$ and the NLRP3 inflammasome pathway in DOX-induced cardiomyopathy remains unclear.

Oxidative stress has recently been widely recognized to be an important factor for DOX-induced cardiomyopathy (21). An imbalance between reactive oxygen species (ROS) and the antioxidant pathway may lead to ROS accumulation in cardiomyocytes. This can then induce damage to mitochondrial membrane proteins and DNA, thereby inhibiting ATP production in mitochondria by disrupting mitochondrial oxidative phosphorylation (22). Increased levels of ROS can cause lipid peroxidation in mitochondria, apoptosis and an excessive inflammatory response in cardiomyocytes, ultimately resulting in cardiac dysfunction (23). A previous study has demonstrated the antioxidant effect of 1,25(OH)$_2$D$_3$ in a number of disease settings, such as osteoporosis (24) and chronic kidney disease (25), in addition to skin senescence (18). Vitamin D3 1α(OH)ase knockout mice demonstrated a significant increase in ROS and H$_2$O$_2$ levels, in addition to aggravation of colon inflammation due to the extensive secretion of senescence-associated inflammatory cytokines (26). A previous study has reported that 1,25(OH)$_2$D$_3$ can activate nuclear erythroid 2-related factor 2 (Nrf2) pathways to activate enhancer of zeste homolog 2-mediated H3K27me^3 histone modification, mediated by EZH2, to regulate downstream target genes (such as p16, p21, p53 and p19) transcriptional expression (27). However, little is known about the mechanism by which 1,25(OH)$_2$D$_3$ regulates DOX-induced cardiomyopathy.

To investigate this issue and its underlying molecular mechanisms, 10-week-old wild-type mice were administered DOX to construct a DOX-induced cardiomyopathy model in the present study. These mice were also administered with 1,25(OH)$_2$D$_3$. Echocardiography, histological and molecular analysis were used to investigate the effect of 1,25(OH)$_2$D$_3$ on DOX-induced cardiomyopathy and its potential mechanism.

Materials and methods

Drugs. DOX (cat. no. A603456) was purchased from Sangon Biotech Co., Ltd. DOX was diluted with normal saline to a concentration of 2 mg/ml for the *in vivo* study and to 43 μM for *in vitro* study. 1,25(OH)$_2$D$_3$ (cat. no. D1530) was purchased from Sigma-Aldrich; Merck KGaA. 1,25(OH)$_2$D$_3$ was diluted with normal saline to a concentration of 0.25 μg/ml for the *in vivo* study and 24 μM for the *in vitro* study.

Animals and experimental procedure. All animal studies were approved by Animal Ethical and Welfare Committee of Nanjing Medical University (approval no. IACUC-1707002) and were performed in accordance with the institutional and national regulations.

C57BL/6J mice (male; n=30; 10 weeks old; 23.81±0.34 g) were purchased from the Model Animal Research Center of Nanjing University and housed at 22-24°C and in a relative humidity of 50±10% under a 12-h light/dark cycle. All the mice had free access to standard chow and water.

The schematic diagram of experimental procedure in the present study is presented in Fig. 1A. After a 1-week acclimation period, mice were randomly divided into three groups (n=10/group). Mice in the DOX-treated group (DOX) were injected intraperitoneally with DOX at a dose of 8 mg/kg per week for 4 weeks and with saline every other day for 4 weeks (28). Mice in the DOX + 1,25(OH)$_2$D$_3$-treated group [DOX + 1,25(OH)$_2$D$_3$] were injected intraperitoneally with DOX at the aforementioned dose and with 1,25(OH)$_2$D$_3$ at a dose of 1 μg/kg every other day for 4 weeks (29). Mice in the Sham group were injected intraperitoneally with saline every other day for 4 weeks. The body weight of each mouse in the Sham, DOX or DOX + 1,25(OH)$_2$D$_3$ groups was measured every week. All mice were sacrificed by CO$_2$ (50% volume replacement rate/min) 4 weeks after the first injection of DOX when echocardiography and serum collection was complete.

The humane endpoints used to determine when animals should be immediately euthanized prior to the scheduled experimental endpoint were as follows: Weight loss of 20%; appetite loss for 24 h or poor appetite (<50% of normal appetite) for 3 days; weakness (inability to eat, drink or stand or extreme difficulty standing); impending death (depressive state with hypothermia); severe diseases of the cutaneous system (uncurable confrontation wound or repetitive self-injury); and severe diseases of the circulatory system (severe hemorrhage or rapid heart rate with marked dyspnea). No mice reached these humane endpoints or died prior to the scheduled experimental endpoint during this 4-week period.

Echocardiography. Echocardiography was performed in the Animal Core Facility of Nanjing Medical University (Nanjing, China) using the high-frequency color ultrasound system (40 μm resolution, 500 frames per second) Vevo 2100 (VisualSonics, Inc.). Cardiac function was evaluated in week 4 after the first injection of DOX was administered. Mice were anesthetized by inhaling isoflurane at a 1:1 concentration with oxygen (4% induction concentration, 1.5% maintenance concentration). Anesthetized mice were fixed in the supine position on a constant-temperature workbench at 25-26°C. Hair on the chest area was removed using a leather knife and
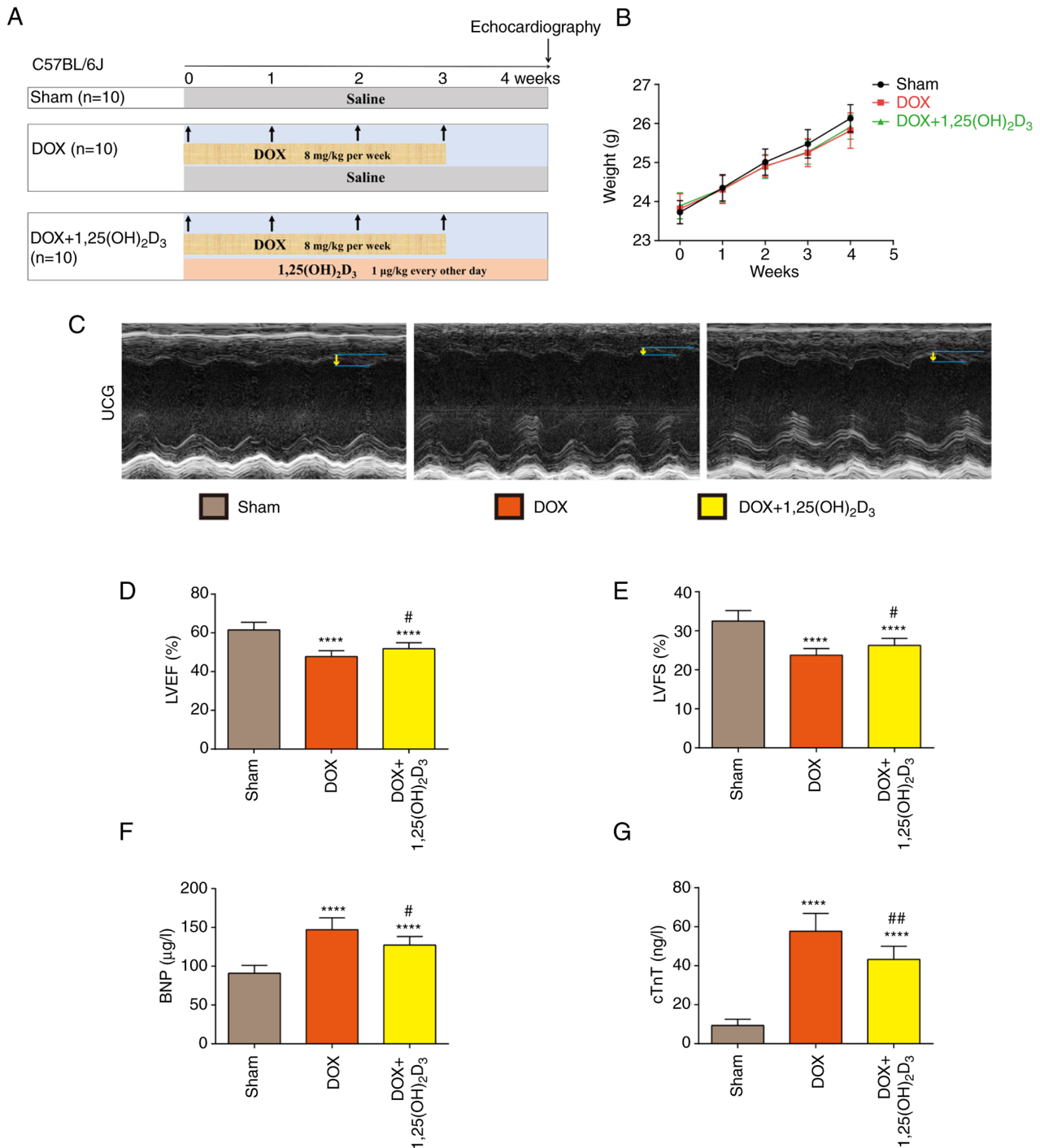
Figure 1. 1,25(OH)$_2$D$_3$ alleviates DOX-induced cardiac dysfunction and injury in mice. (A) Experimental procedure of DOX-induced cardiomyopathy and 1,25(OH$_2$)D$_3$ treatment in C57BL/6J mice. (B) Changes in the body weight of mice in the three treatment groups over 4 weeks. (C) Representative M-mode echocardiograms of mice 4 weeks after the first injection of DOX. Yellow arrow lengths represent the amplitude of ventricular wall motion. (D) LVEF and (E) LVFS as measured using echocardiography (n=8). Levels of (F) BNP and (G) cTnT in serum (n=8). [****]P<0.001 vs. Sham; [#]P<0.05 and [##]P<0.01 vs. DOX. DOX, doxorubicin hydrochloride; UCG, ultrasonic cardiogram; LVEF, left ventricular ejection fraction; LVFS, left ventricular fractional shortening; BNP, brain natriuretic peptide; cTnT, cardiac troponin T.

a simulated electrocardiogram was linked. Left ventricular end-diastolic diameter (LVEDD) and left ventricular end-systolic diameter (LVESD) were measured in the long axis and short axis, respectively. The following formulas were used to calculate left ventricular ejection fraction (LVEF) and left ventricular fractional shortening (LVFS), respectively.

$$\text{LVEF (\%)} = \frac{LVEDD^3 - LVESD^3}{LVEDD^3} \times 100; \ \text{LVFS (\%)} = \frac{LVEDD - LVESD}{LVEDD} \times 100$$

Enzyme-linked immunosorbent assay (ELISA). Serum samples of mice were collected in the Animal Core Facility of Nanjing Medical University in week 4 after the first injection of DOX. Briefly, mice were anesthetized by the intraperitoneal injection of 1% pentobarbital sodium (50 mg/kg), the hair around the eyeball was clipped and blood was then collected by removing the eyeball. A 0.75-ml volume of blood was collected from each mouse. Subsequently, mice were euthanized using CO$_2$. Serum

was obtained by centrifugation (1,500 x g for 10 min at 4˚C) after the blood was left for 1 h at 4˚C for component separation. Brain natriuretic peptide (BNP; cat. no. YFXEM00760) and cardiac troponin T (cTnT; cat. no. YFXEM00789) levels in serum were quantified using ELISA kits (Nanjing Yifeixue Biotechnology Co., Ltd.) according to the manufacturer's protocols.

Measurement of antioxidant enzymes and lipid peroxidation. Myocardial tissues from the left ventricle were prepared as a 10% homogenate with normal saline, followed by centrifugation at 4˚C at 2,000 x g for 15 min. Malondialdehyde (MDA; cat. no. A003-1-1), glutathione peroxidase (GSH-Px; cat. no. A005-1-1) and total superoxide dismutase (T-SOD; cat. no. A001-1-1) in the tissue supernatants were measured using assay kits according to the manufacturer's protocols (Nanjing Jiancheng Bioengineering Institute).

Masson's trichrome staining. Hearts were harvested and fixed in 4% paraformaldehyde at room temperature for 24 h. After standard paraffin embedding (75% alcohol for 4 h, 85% alcohol for 2 h, 90% alcohol for 2 h, 95% alcohol for 1 h, ethyl alcohol I for 30 min, ethyl alcohol II for 30 min, ethyl alcohol and xylene for 10 min, xylene I for 10 min, xylene II for 10 min, 65˚C melted paraffin I for 1 h, 65˚C melted paraffin II for 1 h and 65˚C melted paraffin III for 1 h), heart tissues were cut into 4-μm sequential sections. Masson's trichrome staining (iron hematoxylin for 3 min, lichun red acid fuchsin for 8 min and aniline blue for 5 min, at room temperature) was used to evaluate the degree of myocardial fibrosis. The representative histopathological samples were imaged using a light microscope (Nikon Corporation) and analyzed using Image Pro-Plus software (version 6.0; Media Cybernetics, Inc.). A total of three images from randomly selected non-overlapping fields were captured per section at x400 magnification and the collagen tissue area was expressed as the percentage of the full ventricle area.

Immunohistochemistry. The 4-μm heart paraffin sections were deparaffinized, rehydrated in alcohol (ethyl alcohol for 1 min, 95% alcohol I for 1 min, 95% alcohol II for 1 min and 70% alcohol for 1 min) and washed in tap water. The tissue sections were then boiled for antigen retrieval in a citrate-EDTA antigen retrieval solution (cat. no. P0083; Beyotime Institute of Biotechnology) in a steamer for 30 min at 95-100˚C. Endogenous peroxidase activity was then blocked with methanol and hydrogen peroxide (1:10) for 10 min at room temperature. After washing with TBS (pH 7.6), the sections were blocked with 10% normal goat serum (cat. no. C0265; Beyotime Institute of Biotechnology) for 1 h at room temperature, then incubated with the corresponding primary antibodies overnight at 4˚C. The dilutions of primary antibodies were as follows: IL-1β (cat. no. ab9722; 1 μg/ml; Abcam), IL-6 (cat. no. A0286; 1:200; ABclonal Biotech Co., Ltd.) and TNF-α (cat. no. GTX110520; 1:200; GeneTex, Inc.). After washing with PBS, the sections were incubated with a secondary antibody (MaxVision™ HRP-polymer anti-rabbit IHC kit; ready to use; cat. no. KIT-5004; Fuzhou Maixin Biotech Co., Ltd.) for 30 min at room temperature. Subsequently,

3,3'-diaminobenzidine was used as a chromogen. Finally, tissue sections were counterstained with hematoxylin at room temperature for 3 min and sealed with neutral balsam. The representative histopathological samples (magnification, x400, three random slides/sample) were imaged using a light microscope (Nikon Corporation) and analyzed using Fiji (version 2.3.0), an image processing package based on ImageJ (National Institutes of Health) (30).

Western blotting. Total protein was obtained from left ventricular myocardial tissues by sonication, centrifugation and heat denaturation. Briefly, heart tissues were placed into 4˚C RIPA lysis buffer (cat. No. P0013B; Beyotime Institute of Biotechnology) containing proteinase and phosphatase inhibitors (cat. No. 4906845001; Roche Diagnostics) and phenylmethanesulfonyl fluoride (cat. No. ST506; Beyotime Institute of Biotechnology) for protein extraction. Subsequently, the tissues were homogenized using a FastPrep-24 5G homogenizer (MP Biomedicals, LLC) at 4˚C for 2 min with 4.0-10 m/sec oscillation speed, and was centrifuged at 12,000 x g at 4˚C for 10 min. After quantification using a Pierce BCA Protein Assay Kit (cat. no. PI23225; Thermo Fisher Scientific, Inc.), the supernatant was mixed with loading buffer and heated to 95-100˚C for 5 min. An equal amount (30 μg/lane) of protein was used for western blotting. Proteins were resolved by SDS-PAGE using 8-15 % gradient gels and then transferred onto PVDF membranes. Membranes were blocked with 5 % non-fat milk for 60 min at room temperature and then incubated with the corresponding primary antibodies overnight at 4˚C. The dilutions of primary antibodies used were as follows: Collagen I (cat. No. GTX26308; 1:1,000; GeneTex, Inc.), α-SMA (α-smooth muscle actin; cat. No. ab5694; 1:1,000; Abcam), IL-1β (cat. no. ab9722; 0.25 μg/ml; Abcam), IL-6 (cat. No. A0286; 1:1,000; Abclonal Biotech Co., Ltd.), TNF-α (cat. No. GTX110520; 1:500; GeneTex, Inc.), SOD1 (cat. No. ab16831; 1:2,000; Abcam), SOD2 (cat. No. NB100-1992; 1:2,000; Novus Biologicals, LLC), Nrf2 (cat. No. GTX135165; 1:1,000; GeneTex, Inc.), KEAP1 (Kelch-like ECH-associated protein 1; cat. No. ab119403; 1:1,000; Abcam), Caspase-1 (cat. No. 83383; 1:500; Cell Signaling Technology, Inc.), NLRP3 (cat. No. ab214185; 1:1,000; Abcam), ASC (caspase recruitment domain; cat. No. GTX55818; 1:1,000; GeneTex, Inc.) and GAPDH (cat. No. 2118; 1:1,000; Cell Signaling Technology, Inc.). After washing with TBST (containing 0.25% Tween20), the membrane was incubated with HRP-conjugated goat anti-mouse or anti-rabbit secondary antibodies (cat. No. SA00001-1 or cat. No. SA00001-2; 1:2,000; ProteinTech Group Inc.) for 60 min at room temperature. The membrane was washed three times in TBS with 0.1 % Tween20 (cat. No. ST671; Beyotime Institute of Biotechnology), before being visualized with an enhanced chemiluminescent solution (cat. No. WBKLS0050; MilliporeSigma) and imaged using an Uvitec Alliance mini-chemiluminescence device (Uvitec). GAPDH was used as a loading control. The intensity of the protein bands was quantified using ImageJ software (version 1.44; National Institutes of Health).

Reverse transcription-quantitative polymerase chain reaction (RT-qPCR). RNA was extracted from left ventricular

Table I. Primer sequences used for reverse transcription-quantitative PCR.

Gene target	Forward sequence (5'-3')	Reverse sequence (5'-3')
GAPDH	CCCTTAAGAGGGATGCTGCC	TACGGCCAAATCCGTTCACA
α-SMA	ACATCAAGGAGAAGCTGTGCT	TTTCGTGGATGCCCGCTG
POSTN	TCCCTGATGTCATTACTGATCC	AACCATCTTCAGCCCTGAGC
Fibronectin	ATGAGAAGCCTGGATCCCCT	GGAAGGGTAACCAGTTGGGG
Vimentin	TTCTCTGGCACGTCTTGACC	CTTTCATACTGCTGGCGCAC

α-SMA, α-smooth muscle actin; POSTN, periostin.

myocardial tissues using TRIzol™ Reagent (Invitrogen; Thermo Fisher Scientific, Inc.) and reverse transcription was performed using the 5X All-In-One RT MasterMix (Applied Biological Materials Inc.) according to the manufacturer's protocols. qPCR was performed using the Hieff™ qPCR SYBR® Green Master Mix (Shanghai Yeasen Biotechnology Co., Ltd.) on StepOnePlus Real-Time PCR system (Applied Biosystems; Thermo Fisher Scientific, Inc.) according to the manufacturer's protocol (a two-step amplification: Initial denaturation at 95°C for 5 min, followed by 40 cycles of 95°C for 10 sec and 60°C for 30 sec). Quantification of mRNA was carried out using the $2^{-\Delta\Delta Cq}$ method and normalized to GAPDH [31]. Primer sequences used for the RT-qPCR reactions are presented in Table I.

Cell culture and treatment. Human cardiomyocyte-like AC16 cells were purchased from MilliporeSigma (cat. no. SCC109) and cultured in DMEM (Gibco; Thermo Fisher Scientific, Inc.) containing 10% FBS (Gibco; Thermo Fisher Scientific, Inc.) and 1% penicillin/streptomycin and incubated in 5% CO_2 at 37°C. To model cardiotoxicity *in vitro*, AC16 cells were treated with 1 µM DOX [32] in the absence or presence of 1,25(OH)$_2$D$_3$ for 24 h at 37°C after serum starvation [DOX treatment group or DOX + 1,25(OH)$_2$D$_3$ treatment group, respectively]. Untreated AC16 cells served as the Control group.

Cell viability assays. Cell viability was assayed with the Enhanced Cell Counting Kit (CCK)-8 (Beyotime Institute of Biotechnology) according to the manufacturer's protocols. AC16 cells were seeded into a 96-well plate ($2x10^4$ cells/well) and incubated until adherence was achieved. Cell culture medium was then replaced using DMEM. To evaluate the potential toxicity of 1,25(OH)$_2$D$_3$ towards AC16 cells, AC16 cells were treated with 1,25(OH)$_2$D$_3$ in triplicate at various concentrations (0, 25, 50, 100, 200 and 400 nM) for 24 h at 37°C. To evaluate the protective effects of 1,25(OH)$_2$D$_3$ against DOX-induced cytotoxicity, AC16 cells were treated with 1 µM DOX and various concentrations of 1,25(OH)$_2$D$_3$ (0, 25, 50, 100 and 200 nM) in triplicate for 24 h at 37°C. Subsequently, 10 µl enhanced CCK-8 solution was added into each well, cells were incubated for 2 h at 37°C and the absorbance at 450 nm was measured.

ROS analysis. ROS production in AC16 cells was assessed using 2',7'-dichlorofluorescin diacetate (DCFH-DA; cat. no. 35845; MilliporeSigma). Following starvation treatment and induction of cardiotoxicity, AC16 cells were incubated with 10 µM DCFH-DA in the dark at 37°C for 30 min and then washed twice with PBS. Oxidized 2',7'-dichlorofluorescin fluorescence (representing ROS level) was detected immediately by fluorescent microscopy (Guangzhou Micro-shot Technology Co., Ltd.). A total of three images from randomly selected non-overlapping fields were captured and the intensity of fluorescence was quantified using ImageJ software (version 1.44; National Institutes of Health).

Chromatin immunoprecipitation (ChIP) assay. AC16 cells were collected for ChIP assay using the High-Sensitivity ChIP kit (cat. no. 9003; Cell Signaling Technology, Inc.) following the manufacturer's protocol. H2AK119Ub (cat. no. 8240), H3K4me^3 (cat. no. 9751) and H3K27me^3 (cat. no. 9733) were purchased from Cell Signaling Technology Inc., which were used for the ChIP assay. Briefly, two 10-cm dishes containing $1x10^7$ cells in 10 ml culture media were used for each ChIP experiment. Cells were crosslinked with 1% formaldehyde for 10 min at room temperature on an orbital shaker (60 rpm). The formaldehyde was then quenched by adding glycine (75 mM), the cells were incubated at room temperature for 10 min and rinsed twice with PBS. Cells were scraped and transferred into 15-ml Falcon tubes, before being centrifuged at 350 x g for 5 min at 4°C. Cells were resuspended in 15 ml Buffer A [20 mM HEPES (pH=7.4), 10 mM EDTA, 0.5 mM EGTA and 0.25% Triton X-100] and incubated at 4°C for 5 min. The cells were then centrifuged at 350 x g for 5 min at 4°C and resuspended in 15 ml Buffer B [20 mM HEPES (pH=7.4), 150 mM NaCl, 10 mM EDTA and 0.5 mM EGTA] and incubated at 4°C for 5 min on a rotating wheel. Cells were centrifuged again at 350 x g for 5 min at 4°C and resuspended in 1 ml Buffer C [20 mM HEPES (pH=7.4), 10 mM EDTA, 0.5 mM EGTA, 0.1% SDS and 1X Protease Inhibitor Cocktail (cat. no. #5871; Cell Signaling Technology). After incubating for 10 min on ice, the cells were transferred into a 15-ml sonication tube. Sonication was performed using a Bioruptor (Bioruptor PLUS; Diagenode S.A.) using the following protocol: 10 Cycles of 30-sec sonication (150 Hz, at 4°C), followed by 20 sec off, at high power for a total of 20 cycles with a 10-min pause and incubation on ice every 10 cycles. The sonicated chromatin was centrifuged at 16,000 x g for 10 min at 4°C. For each immunoprecipitation reaction, chromatin (10 µg DNA), measured via Nanodrop2000 (Thermo Fisher Scientific, Inc.), was diluted to a total of 500 µl with 1X ChIP Buffer + PIC. Next, 5 µg antibodies were added into chromatin (10 µg DNA)

Table II. Primer sequences used for chromatin immunoprecipitation.

Gene target	Forward sequence (5'-3')	Reverse sequence (5'-3')
NLRP3	GGGACCAAATTGAGGGCTTC	TCAACGTCACCAGTCCTCAGA
Nrf2	AGAATGAATGGCCTCCAGCC	CATTACCATGCCCCCAGAGG

NLRP3, nod-like receptor family pyrin domain containing 3; Nrf2, nuclear erythroid 2-related factor 2.

in 500 μl 1X ChIP Buffer + PIC. Immunoprecipitated samples were incubated on an oscillating platform at 4°C overnight. The following day, 30 μl Protein G Magnetic Beads were added immediately into each immunoprecipitation reaction and incubated on an oscillating platform at 4°C for 2 h. Each sample tube was placed on a magnetic separator for 2 min to precipitate the Protein G Magnetic Beads until the solution was cleared and the supernatant was removed. The protein G magnetic beads were then washed using low- and high-salt wash. They were then re-suspended in 150 μl 1X ChIP eluting buffer before the chromatin was eluted from the samples using a vortex (200 x g at 65°C for 30 min). Samples were centrifuged at 10,000 x g at 4°C for 10 sec to remove trace amounts of evaporated sample from the centrifuge tube cap. The eluted chromatin supernatant was then transferred to a new tube. Un-crosslinking was performed by adding 6 μl 5M NaCl and 2 μl Proteinase K to each sample and incubating at 65°C for 2 h. DNA Binding Buffer (750 μl) was added to each DNA sample and swirled to mix, before 450 μl sample was transferred to a DNA centrifuge column in the collection tube and centrifuged at 16,000 x g at 4°C for 30 sec. DNA Wash Buffer (750 μl) was added to the centrifuge column in the collection tube and the samples were centrifuged again at 16,000 x g at 4°C for 30 sec. DNA Elution Buffer (50 μl) was added to each centrifuge column, placed in a clean 1.5-ml microcentrifuge tube and centrifuged at 16,000 x g at 4°C for 30 sec to elute the DNA. The eluate was purified for subsequent qPCR assay. DNA purification was performed as described in the Chip kit instructions (cat. no. 9003; Cell Signaling Technology, Inc.). qPCR was performed using the Hieff™ qPCR SYBR® Green Master Mix (Shanghai Yeasen Biotechnology Co., Ltd.) on StepOnePlus Real-Time PCR system (Applied Biosystems; Thermo Fisher Scientific, Inc.) according to the manufacturer's protocol (a two-step amplification: Initial denaturation at 95°C for 5 min, followed by 40 cycles of 95°C for 10 sec and 60°C for 30 sec). Quantification of mRNA was carried out using the $2^{-\Delta\Delta Cq}$ method and normalized to input. In this experiment, the qPCR method was used to quantify the Chip experiment. The enrichment level was calculated by the formula 2% x 2 [C(T) 2% input-C(T) IP sample] with reference to operating instructions of the Chip kit (cat. no. 9003; Cell Signaling Technology, Inc.). For DNA gel assay, 2 X Taq Master Mix (Dye Plus) (Vazyme, P112-01) was used for PCR assay. The following DNA amplification procedure was applied: i) Initial denaturation 95°C for 5 min; ii) denaturation 95°C for 30 sec; ii) refolding at 62°C for 30 sec; iv) extension at 72°C for 30 sec; v) repeat of step ii)-iv) for 34 cycles; and vi) terminal extension at 72°C for 5 min. DNA products were detected using 2% agarose gel electrophoresis. GelDoc XR System (Bio-Rad) was used for gel imaging. Primer sequences used for ChIP-qPCR reactions are presented in Table II.

Statistical analysis. Data from ≥ three independent experiments were expressed as the mean ± standard deviation. All statistical analyses were performed using the GraphPad Prism software (version 7.0; GraphPad Software, Inc.; Dotmatics). Statistical differences among treatment groups were analyzed using a one-way ANOVA followed by Tukey's test. P<0.05 was considered to indicate a statistically significant difference.

Results

1,25(OH)$_2$D$_3$ alleviates DOX-induced cardiac dysfunction and injury. Mice were administered with DOX to construct a DOX-induced cardiomyopathy model whilst 1,25(OH)$_2$D$_3$ was administered to mice as previously described (Fig. 1A). The body weight of each mouse in the Sham, DOX and DOX + 1,25(OH)$_2$D$_3$ groups were measured each week, which yielded no significant differences among the three treatment groups (Fig. 1B). Echocardiography images of mice on week 4 indicated that ventricular wall motion amplitude markedly decreased after DOX administration, which was alleviated by 1,25(OH)$_2$D$_3$ (Fig. 1C). LVEF and LVFS were observed to be significantly decreased after DOX administration compared with those in the sham group (Fig. 1D and E). Compared with those in the DOX-treated group, 1,25(OH)$_2$D$_3$ treatment significantly increased LVEF and LVFS (Fig. 1D and E). Treatment with 1,25(OH)$_2$D$_3$ also significantly reduced the serum levels of BNP in mice with DOX-induced cardiomyopathy (Fig. 1F). Analysis of cTnT levels in serum was performed to detect signs of myocardial injury, which demonstrated that cTnT levels were significantly increased after DOX administration compared with those in the Sham group, which was in turn significantly reversed by 1,25(OH)$_2$D$_3$ treatment (Fig. 1G). These results suggest that 1,25(OH)$_2$D$_3$ treatment can alleviate DOX-induced cardiac dysfunction and injury.

1,25(OH)$_2$D$_3$ inhibits the activation of a pro-fibrotic and inflammatory microenvironment in DOX-induced cardiomyopathy. As 1,25(OH)$_2$D$_3$ was found to alleviate DOX-induced cardiac dysfunction and injury, it was therefore hypothesized that 1,25(OH)$_2$D$_3$ may reverse the fibrotic and inflammatory microenvironment in a model of DOX-induced cardiomyopathy. Masson's trichrome staining was used to evaluate the extent of myocardial fibrosis. 1,25(OH)$_2$D$_3$ was demonstrated to significantly inhibit collagen deposition in the heart tissues of mice with DOX-induced cardiac dysfunction (Fig. 2A and B). The mRNA expression levels of α-SMA, periostin (POSTN),
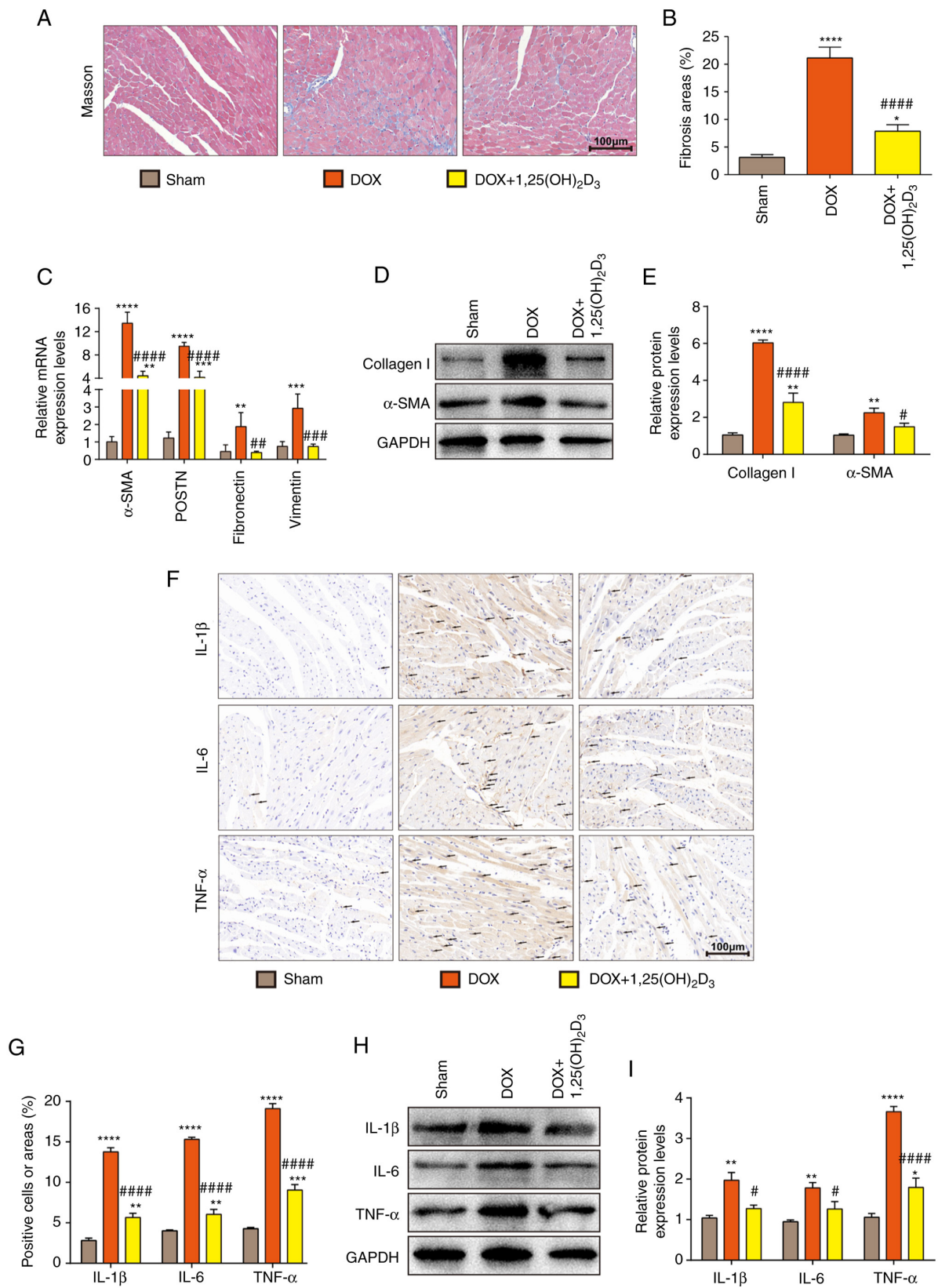
Figure 2. 1,25(OH)$_2$D$_3$ inhibits the activation of a pro-fibrotic and inflammatory microenvironments in DOX-induced cardiomyopathy in mice. (A) Representative images of Masson's trichrome staining of cardiac tissue and (B) quantification of fibrosis (n=3). (C) Relative mRNA expression levels of α-SMA, POSTN, fibro-nectin and vimentin in cardiac tissues (n=5). (D) Western blotting images of cardiac tissue extracts for protein expression of collagen I and α-SMA. GAPDH was used as the loading control. (E) Semi-quantification of protein expression levels of collagen I and α-SMA. Protein expression levels relative to Sham group were assessed by densitometric analysis (n=3). (F) Representative images of immunohistochemical staining for IL-1β, IL-6 and TNF-α. Black arrows indicate areas of positive expression. (G) Percentage of cells or areas positive for IL-1β, IL-6 and TNF-α relative to number of total cells or areas (n=3). (H) Western blotting images of cardiac tissue extract for the protein expression of IL-1β, IL-6 and TNF-α. GAPDH was used as the loading control. (I) Semi-quantification of protein expression levels of IL-1β, IL-6 and TNF-α. Protein expression levels relative to Sham group were assessed by densitometric analysis (n=3). *P<0.05, **P<0.01, ***P<0.001 and ****P<0.0001 vs. Sham; $^#$P<0.05, $^{##}$P<0.01, $^{###}$P<0.001 and $^{####}$P<0.0001 vs. DOX. DOX, doxorubicin hydrochloride; α-SMA, α-smooth muscle actin; POSTN, periostin.

Fibronectin and Vimentin in mice with DOX-induced cardiomyopathy were also found to be significantly reduced after 1,25(OH)$_2$D$_3$ treatment (Fig. 2C). In addition, it was demonstrated through western blotting that 1,25(OH)$_2$D$_3$ significantly downregulated α-SMA and collagen I protein expression levels compared with those in the DOX group (Fig. 2D and E). These results suggest the anti-fibrotic effect of 1,25(OH)$_2$D$_3$ against DOX-induced cardiomyopathy.

Immunohistochemistry staining was subsequently used to examine whether 1,25(OH)$_2$D$_3$ can reduce the production of inflammatory mediators in DOX-induced cardiomyopathy. The results demonstrated that the expression levels of IL-1β, IL-6 and TNF-α were significantly decreased in the DOX + 1,25(OH)$_2$D$_3$-treated group compared with those in the DOX-treated group (Fig. 2F and G). These findings were confirmed by western blotting, which demonstrated significantly reduced IL-1β, IL-6 and TNF-α protein expression levels in mice with DOX-induced cardiomyopathy treated with 1,25(OH)$_2$D$_3$ (Fig. 2H and I). These results suggest that 1,25(OH)$_2$D$_3$ inhibited the activation of a pro-fibrotic and inflammatory microenvironment in a mouse model of DOX-induced cardiomyopathy.

Increases in oxidative stress and the NLRP3 inflammasome pathways are ameliorated by 1,25(OH)$_2$D$_3$ treatment in DOX-induced cardiomyopathy. Although 1,25(OH)$_2$D$_3$ inhibited the activation of a pro-fibrotic and inflammatory microenvironment, the detailed mechanism underlying the regulation of this process remain poorly understood. Previous studies have reported that mitochondrial dysfunction and excessive activation of oxidative stress can aggravate DOX-induced cardiomyopathy (33,34). Furthermore, another previous study demonstrated that 1,25(OH)$_2$D$_3$ can significantly inhibit the production of ROS in skin and liver senescent cells (18). It was therefore hypothesized that 1,25(OH)$_2$D$_3$ administration could inhibit oxidative stress. Consequently, the associated pathway in DOX-induced cardiomyopathy was next assessed. To clarify this hypothesis, cell viability was analyzed using the CCK-8 kit to determine the minimal treatment concentration of 1,25(OH)$_2$D$_3$ that can cause toxicity in AC16 cells. CCK-8 results demonstrated that cell viability was not affected upon treatment with different concentrations of 1,25(OH)$_2$D$_3$ (0, 25, 50, 100, 200 and 400 nM), suggesting that no cytotoxicity to 1,25(OH)$_2$D$_3$ was demonstrated in AC16 cells up to a dose of 400 nM (Fig. 3A). Cell viability was found to be significantly decreased when the AC16 cells were treated with DOX (Fig. 3B). Doses of 50, 100 and 200 nM 1,25(OH)$_2$D$_3$ exhibited a significant protective effect against DOX-induced cytotoxicity in AC16 cells (Fig. 3B). In particular, the 100 and 200 nM doses of 1,25(OH)$_2$D$_3$ exhibited significantly increased protective effects on cell viability compared with that after treatment with the 50 nM dose of 1,25(OH)$_2$D$_3$ (Fig. 3B). Doubling the 1,25(OH)$_2$D$_3$ concentration to 200 nM had no significant effects on cell viability compared with that after 100 nM 1,25(OH)$_2$D$_3$ treatment (Fig. 3B). Therefore, 100 nM 1,25(OH)$_2$D$_3$ was selected as the safe and effective treatment dose for subsequent experiments.

Intracellular ROS levels in AC16 cells were analyzed using DCFH-DA staining, which demonstrated that DOX treatment significantly increased the intracellular ROS levels compared with those in control cells (Fig. 3C and D). Treatment of AC16 cells with 100 nM 1,25(OH)$_2$D$_3$ significantly decreased intracellular ROS levels compared with cells treated with DOX only (Fig. 3C and D). Oxidative stress was also measured in cardiac tissue homogenates of mice on the 4th week after the first injection of DOX was administered. Compared with those in the Sham group, cardiac tissues from DOX-treatment mice demonstrated a significantly increased MDA level but decreased T-SOD and GSH-Px levels (Fig. 3E-G). Mice in the DOX + 1,25(OH)$_2$D$_3$-treated group demonstrated significantly lower MDA levels, but markedly higher T-SOD and significantly higher GSH-Px levels, compared with those in the DOX-treated group (Fig. 3E-G). To further determine the potential mechanism of action underlying this process, protein expression levels of KEAP1, Nrf2, SOD1 and SOD2 were analyzed using western blotting. Compared with those in the DOX-treated group, 1,25(OH)$_2$D$_3$ treatment significantly increased SOD1, SOD2 and Nrf2 protein expression, whilst significantly decreasing KEAP1 expression (Fig. 3H and I). Taken together, these results suggest that 1,25(OH)$_2$D$_3$ reduced oxidative stress in DOX-induced cardiomyopathy by inhibiting the KEAP1/Nrf2 pathway.

The NLRP3 inflammasome has received considerable attention in the field of inflammation research (35,36). Levels of NLRP3 inflammasome-associated proteins in DOX-induced cardiomyopathy mice were therefore next analyzed, which demonstrated that the protein expression levels of NLRP3, ASC and Caspase-1 were significantly decreased with 1,25(OH)$_2$D$_3$ treatment compared with those in the DOX-only treatment group (Fig. 3J and K).

Taken together, these results suggested that 1,25(OH)$_2$D$_3$ ameliorated oxidative stress and inhibited the NLRP3 inflammasome pathway to alleviate the pathophysiological processes associated with DOX-induced cardiomyopathy.

1,25(OH)$_2$D$_3$ treatment affects histone modification levels in NLRP3 and Nrf2 promoters in DOX-induced cardiomyopathy. Previous studies have reported that 1,25(OH)$_2$D$_3$ can affect histone modifications to regulate downstream target gene expression and impact transcriptional regulation (37). To clarify the effect of 1,25(OH)$_2$D$_3$ on the level of histone modification in the NLRP3 promoter, ChIP assay was used to assess the levels of H3K4 (H3K4me^3) and H3K27 (H3K27me^3) trimethylation, in addition to H2AK119 monoubiquitination (H2AK119Ub), in the NLRP3 promoter region. The results demonstrated that 1,25(OH)$_2$D$_3$ treatment significantly decreased the level of H3K4me^3 whilst significantly increasing the levels of H3K27me^3 and H2AK119Ub in the NLRP3 promoter region, compared with that in the DOX-treated group (Figs. 4A-C and S1A). H3K4me^3 modification may loosen chromatin and activate transcriptional expression (38). By contrast, H3K27me^3 and H2AK119Ub modification may cause chromatin compression and inhibit the transcription of downstream genes (39). These results suggested that the inhibition of NLRP3 transcription by 1,25(OH)$_2$D$_3$ may have occurred due to a decrease in the levels of histone modification that is conducive to transcription activation and an increase in the levels of histone modifications that favor transcriptional inhibition in the NLRP3 promoter region.
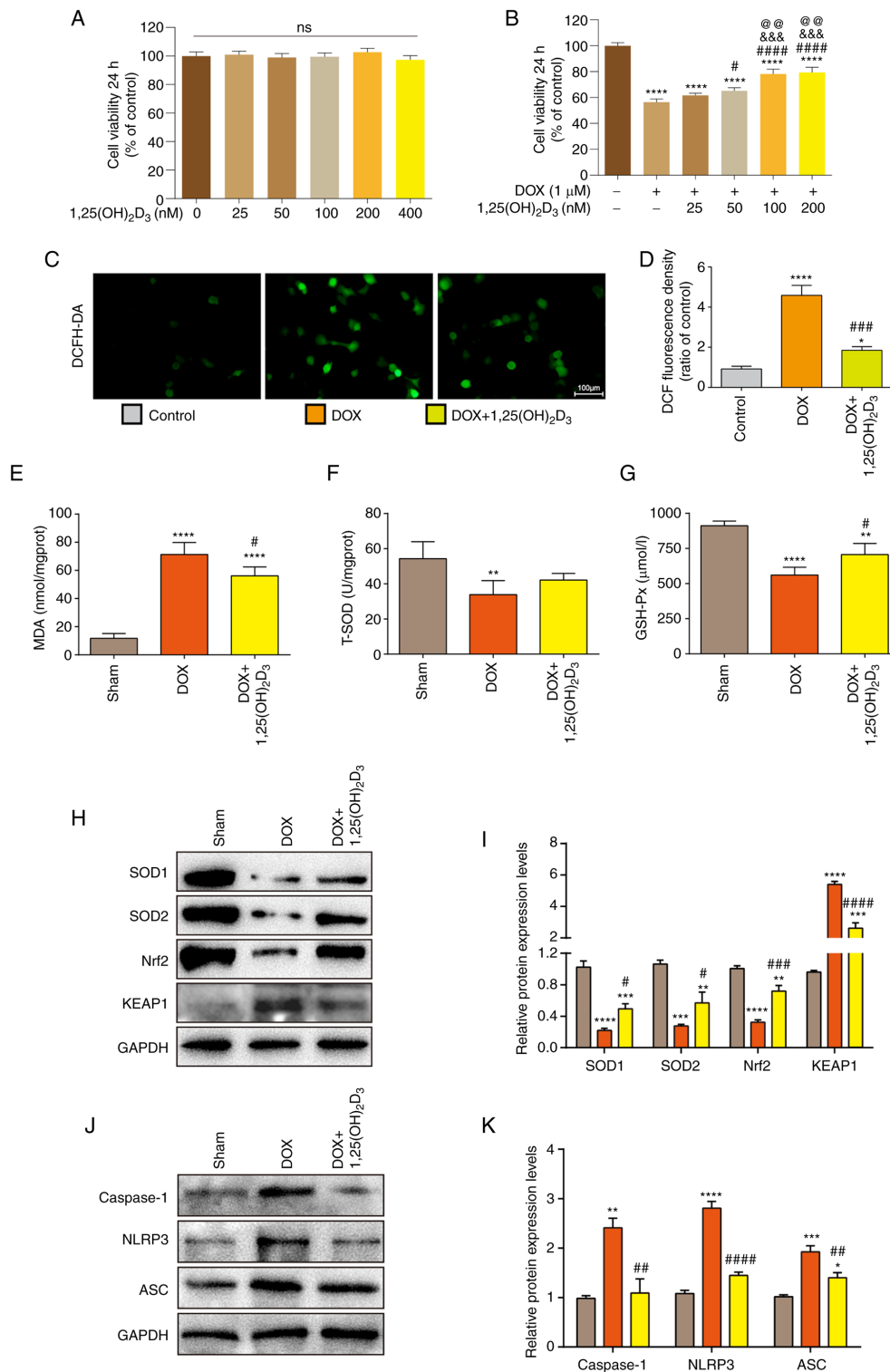
Figure 3. Increased oxidative stress and NLRP3 inflammasome pathways are ameliorated by 1,25(OH)$_2$D$_3$ treatment in DOX-induced cardiomyopathy in mice. (A) AC16 cells treated with different concentrations of 1,25(OH)$_2$D$_3$ (0, 25, 50, 100, 200 and 400 nM) for 24 h. Cell viability was measured using CCK-8 assay (n=3). (B) AC16 cells were treated with 1 μM DOX and different concentrations of 1,25(OH)$_2$D$_3$ (0, 25, 50, 100 and 200 nM) for 24 h. Cell viability was measured using CCK-8 assay (n=3). ****P<0.0001 vs. Control group; #P<0.05 and ####P<0.0001 vs. DOX-only group; &&&P<0.001 vs. DOX + 25 nM 1,25(OH)$_2$D$_3$-treated group; @@P<0.01 vs. DOX + 50 nM 1,25(OH)$_2$D$_3$-treated group. (C) Levels of reactive oxygen species and (D) densitometric analysis in AC16 cells after treatment with DOX or DOX + 1,25(OH)$_2$D$_3$ via DCFH-DA staining (n=5). *P<0.05 and ****P<0.0001 vs. Control; ###P<0.001 vs. DOX group. Levels of (E) MDA, (F) T-SOD and (G) GSH-Px in cardiac tissue 4 weeks after the first injection of DOX (n=5). (H) Western blotting images of cardiac tissue extracts analyzing protein expression of SOD1, SOD2, Nrf2 and KEAP1. GAPDH was used as the loading control. (I) Semi-quantification of protein expression levels of SOD1, SOD2, Nrf2 and KEAP1. Protein expression levels relative to the Sham group were assessed by densitometric analysis (n=3). (J) Western blotting images of cardiac tissue extracts analyzing protein expression of NLRP3, ASC and Caspase-1. GAPDH was used as the loading control. (K) Semi-quantification of protein expression levels NLRP3, ASC and Caspase-1. Protein expression levels relative to the Sham group were assessed by densitometric analysis (n=3). *P<0.05, **P<0.01, ***P<0.001 and ****P<0.0001 vs. Sham; #P<0.05, ##P<0.01, ###P<0.001 and ####P<0.001 vs. DOX. DOX, doxorubicin hydrochloride; CCK-8, Cell Counting Kit-8; ns, no significant difference; DCFH-DA, 2',7'-dichlorofluorescin diacetate; MDA, malondialdehyde; T, total; GSH-Px, glutathione peroxidase; SOD, superoxide dismutase; Nrf2, nuclear erythroid 2-related factor 2; KEAP1, Kelch-like ECH-associated protein 1; ASC, caspase recruitment domain; NLRP3, nod-like receptor family pyrin domain-containing 3 inflammasome.
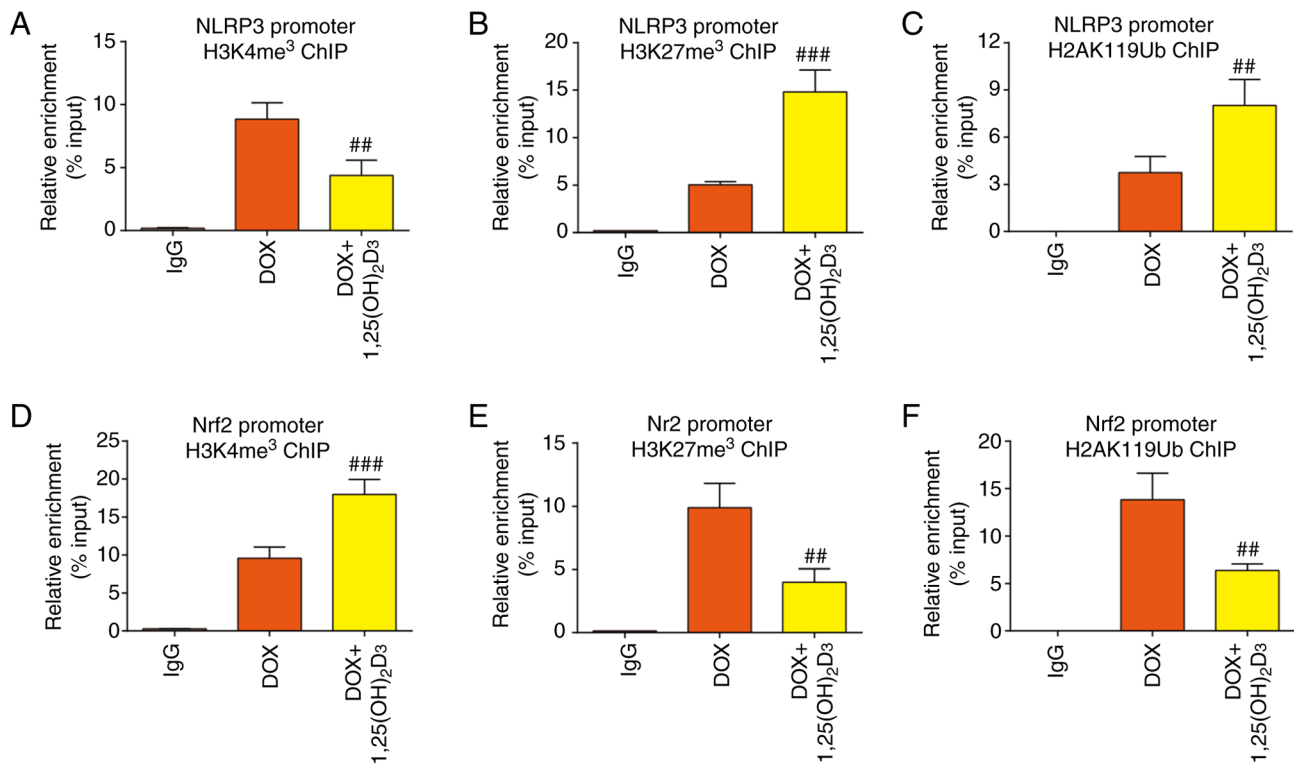
Figure 4. 1,25(OH)$_2$D$_3$ treatment affects histone modification levels in NLRP3 and Nrf2 promoters in DOX-induced cardiomyopathy. Binding levels of (A) H3K4me^3, (B) H3K27me^3 and (C) H2AK119Ub in the NLRP3 promoter region in AC16 cells after treatment with DOX or DOX + 1,25(OH)$_2$D$_3$, detected using ChIP assay (n=5). Binding levels of (D) H3K4me^3, (E) H3K27me^3 and (F) H2AK119Ub in the Nrf2 promoter region in AC16 cells after treatment with DOX or DOX + 1,25(OH)$_2$D$_3$, detected using ChIP assay (n=5). $^{##}$P<0.01 and $^{###}$P<0.001 vs. DOX. DOX, doxorubicin hydrochloride; NLRP3, nod-like receptor family pyrin domain-containing 3; Nrf2, nuclear erythroid 2-related factor 2; ChIP, chromatin immunoprecipitation.

The levels of different histone modifications in the Nrf2 promoter region were also evaluated. Treatment with 1,25(OH)$_2$D$_3$ significantly increased the level of H3K4me^3 whilst significantly decreasing the levels of H3K27me^3 and H2AK119Ub in the Nrf2 promoter region in a model of DOX-induced cardiomyopathy, suggesting that 1,25(OH)$_2$D$_3$ stimulation increased the transcriptional level of Nrf2 (Figs. 4D-F and S1B). These results contrast with those observed in the NLRP3 promoter. Therefore, these data suggest that 1,25(OH)$_2$D$_3$ treatment could significantly affect chromatin accessibility in cardiomyocytes to participate in the progression of cardiomyopathy, but the regulation of this process is likely to be complex.

Discussion

DOX, an anthracycline antibiotic derived from *Streptomyces*, is widely used for the treatment of multiple types of cancer, such as leukemia, lung and breast cancer (40). However, the toxic effects of DOX on cardiomyocytes limits its clinical application (3). The pathogenesis of DOX-induced cardiomyopathy remains poorly understood and there is a lack of effective therapeutic drugs (7). Therefore, it is particularly important to explore its mechanism and search for potential and effective treatment.

1,25(OH)$_2$D$_3$ is a metabolic derivative of vitamin D3 and its production needs catalysis by the CYP27B1 enzyme (9). 1,25(OH)$_2$D$_3$ binds to the vitamin D receptor (VDR) to induce downstream effects, such as anti-oxidative stress and anti-cell senescence (17,18). VDR and CYP27B1 are expressed in multiple organ and cell types, including the heart, suggesting that the targets of 1,25(OH)$_2$D$_3$ are wide-ranging (41). Previous studies have reported that 1 μg/kg 1,25(OH)$_2$D$_3$ exhibits antioxidant and anti-inflammatory effects on certain organs, such as the skin, liver and kidneys, in addition to impacting a number of diseases, such as arthrosis (by promoting apoptosis of fibroblast-like synoviocytes) and breast cancer (by inhibiting oxidative stress and inducing tumor cellular senescence) in mice (18,29,42). Oxidative stress and inflammation can also serve vital roles in DOX-induced cardiomyopathy (34). However, a potential risk of vitamin D overproduction is that it can cause high calcium and phosphorus levels, which are harmful to health, resulting in hyperparathyroidism, vascular calcification and arrhythmia (43). Previous studies have reported that 1 μg/kg 1,25(OH)$_2$D$_3$ has no effect on serum levels of calcium and phosphorus in mice, suggesting that 1 μg/kg can be used as a safe dose in mouse studies (18,29). Considering the impact of 1,25(OH)$_2$D$_3$ on multiple organ systems and the safety data reported in previous studies (18,29,42), the aforementioned dose (1 μg/kg) was used to study the potential effects of 1,25(OH)$_2$D$_3$ in a mouse model of DOX-induced cardiomyopathy.

The present study demonstrated that 1,25(OH)$_2$D$_3$ treatment could increase the levels of H3K27me^3 and H2AK119Ub and decrease the level of H3K4me^3 in the NLRP3 promoter region in DOX-induced cardiomyopathy. By contrast, treatment with 1,25(OH)$_2$D$_3$ decreased the levels of H3K27me^3 and H2AK119Ub and increased the level of H3K4me^3 in the Nrf2

promoter region. Therefore, $1,25(OH)_2D_3$ may inhibit the activation of the NLRP3 inflammasome and KEAP1/Nrf2-induced oxidative stress, in turn alleviating the pathophysiological processes of DOX-induced cardiomyopathy.

The NLRP3 inflammasome is an important part of the inflammasome family and serves a critical role in inflammatory responses to multiple exogenous and endogenous factors (35). The NLRP3 inflammasome contains an NLRP3 protein that interacts with its adapter apoptosis-associated speck-like protein containing an ASC to recruit and activate caspase-1, which processes pro-IL-1β to mature IL-1β to trigger an inflammatory response (44). Cao *et al* (45) previously reported that $1,25(OH)_2D_3$ can alleviate colitis disease progression by inhibiting the NLRP3 pathway, which is consistent with findings of the present study. The present study also demonstrated the inhibitory effect of $1,25(OH)_2D_3$ on the NLRP3 inflammasome pathway in DOX-induced cardiomyopathy. However, Tulk *et al* (46) reported that $1,25(OH)_2D_3$ can enhance the secretion of IL-1β in THP-1 cells by activating the NLRP3 inflammasome pathway after phorbol 12-myristate 13-acetate stimulation. Conflicting results obtained using different cell lines suggest that $1,25(OH)_2D_3$ may serve different roles depending on the cell type or under different pathological conditions, further indicating the complex role of $1,25(OH)_2D_3$ in different cell types.

Epigenetic modification serves as another regulatory process of gene transcription (47,48). Epigenetic regulation mechanisms, including CpG island DNA methylation, histone modification and non-coding RNA regulation, are considered key to regulating the transcription of the NLRP3 inflammasome (49). Lecoeur *et al* (50) reported that NLRP3 promoters exhibit a high level of histone H3K9/14 deacetylation and a high level of histone H3K4 demethylation during *Leishmania amazonensis* infection. As an important type of histone modification, histone ubiquitination also serves an important role in transcriptional regulation (39). Histone ubiquitination has been reported to serve an important role in DNA damage repair (51), stem cell regulation (52) and DNA replication (53). Previous studies have reported that $1,25(OH)_2D_3$ can increase the level of $H3K9me^2$ in the bone morphogenic protein 2 (BMP2) promoter region and regulates the transcriptional expression of the BMP2 gene through binding to VDR (54,39). However, to the best of our knowledge, no studies have assessed whether $1,25(OH)_2D_3$ can affect histone modifications in the NLRP3 promoter region. In the present study, it was demonstrated that $1,25(OH)_2D_3$ decreased $H3K4me^3$ levels whilst increasing $H3K27me^3$ and H2AK119Ub levels in the NLRP3 promoter region. A decrease in the levels of histone modifications favoring transcriptional activation and an increase in the levels of histone modifications favoring transcriptional inhibition can lead to significant chromatin compression in the NLRP3 promoter region to inhibit transcription.

In conclusion, the present study demonstrated that $1,25(OH)_2D_3$ can regulate histone modification in NLRP3 and Nrf2 promoters, inhibit activation of the NLRP3 inflammasome pathway and oxidative stress in cardiomyocytes, in addition to alleviating the pathophysiological processes of DOX-induced cardiomyopathy. Therefore, $1,25(OH)_2D_3$ may serve to be a future potential therapeutic drug for the treatment of DOX-induced cardiomyopathy.

Availability of data and materials

The datasets used and/or analyzed during the current study are available from the corresponding author on reasonable request.

Authors' contributions

XG, XW, YD and JZ contributed to study conception and design. XG, LZ, JY, LC, CS and BL performed experiments. XG, LZ, JY and XW generated figures and performed data analysis. XG and YD confirm the authenticity of all the raw data. All authors read and approved the final version of the manuscript.

Ethics approval and consent to participate

All animal studies were approved by Animal Ethical and Welfare Committee of Nanjing Medical University (approval no. IACUC-1707002).

Patient consent for publication

Not applicable.

Competing interests

The authors declare that they have no competing interests.

References

1. Wang AJ, Tang Y, Zhang J, Wang BJ, Xiao M, Lu G, Li J, Liu Q, Guo Y and Gu J: Cardiac SIRT1 ameliorates doxorubicin-induced cardiotoxicity by targeting sestrin 2. Redox Biol 52: 102310, 2022.
2. Kabir S, Lingappa N and Mayrovitz H: Potential therapeutic treatments for doxorubicin-induced cardiomyopathy. Cureus 14: e21154, 2022.
3. Schirone L, D'Ambrosio L, Forte M, Genovese R, Schiavon S, Spinosa G, Iacovone G, Valenti V, Frati G and Sciarretta S: Mitochondria and doxorubicin-induced cardiomyopathy: A complex interplay. Cells 11: 2000, 2022.

4. Baker LH, Boonstra PS, Reinke DK, Antalis E, Zebrack BJ and Weinberg RL: Burden of chronic diseases among sarcoma survivors treated with anthracycline chemotherapy: Results from an observational study. J Cancer Metastasis Treat 6: 24, 2020.

5. Suzuki K, Murtuza B, Suzuki N, Smolenski RT and Yacoub MH: Intracoronary infusion of skeletal myoblasts improves cardiac function in doxorubicin-induced heart failure. Circulation 104: I213-I217, 2001.

6. Deng S, Kulle B, Hosseini M, Schluter G, Hasenfuss G, Wojnowski L and Schmidt A: Dystrophin-deficiency increases the susceptibility to doxorubicin-induced cardiotoxicity. Eur J Heart Fail 9: 986-994, 2007.

7. Chen Y, Shi S and Dai Y: Research progress of therapeutic drugs for doxorubicin-induced cardiomyopathy. Biomed Pharmacother 156: 113903, 2022.

8. Christakos S, Dhawan P, Verstuyf A, Verlinden L and Carmeliet G: Vitamin D: Metabolism, molecular mechanism of action, and pleiotropic effects. Physiol Rev 96: 365-408, 2016.

9. Carlberg C and Munoz A: An update on vitamin D signaling and cancer. Semin Cancer Biol 79: 217-230, 2022.

10. Malluche HH, Henry H, Meyer-Sabellak W, Sherman D, Massry SG and Norman AW: Effects and interactions of 24R,25(OH)2D3 and 1,25(OH)2D3 on bone. Am J Physiol 238: E494-E498, 1980.

11. Carlberg C: Vitamin D signaling in the context of innate immunity: Focus on human monocytes. Front Immunol 10: 2211, 2019.

12. Chanakul A, Zhang MY, Louw A, Armbrecht HJ, Miller WL, Portale AA and Perwad F: FGF-23 regulates CYP27B1 transcription in the kidney and in extra-renal tissues. PLoS One 8: e72816, 2013.

13. Ismailova A and White JH: Vitamin D, infections and immunity. Rev Endocr Metab Disord 23: 265-277, 2022.

14. de la Guia-Galipienso F, Martinez-Ferran M, Vallecillo N, Lavie CJ, Sanchis-Gomar F and Pareja-Galeano H: Vitamin D and cardiovascular health. Clin Nutr 40: 2946-2957, 2021.

15. Guo X, Lin H, Liu J, Wang D, Li D, Jiang C, Tang Y, Wang J, Zhang T, Li Y, *et al*: 1,25-Dihydroxyvitamin D attenuates diabetic cardiac autophagy and damage by vitamin D receptor-mediated suppression of FoxO1 translocation. J Nutr Biochem 80: 108380, 2020.

16. Samefors M, Scragg R, Lanne T, Nyström FH and Östgren CJ: Association between serum 25(OH)D3 and cardiovascular morbidity and mortality in people with type 2 diabetes: A community-based cohort study. Diabet Med 34: 372-379, 2017.

17. Cui C, Xu P, Li G, Qiao Y, Han W, Geng C, Liao D, Yang M, Chen D and Jiang P: Vitamin D receptor activation regulates microglia polarization and oxidative stress in spontaneously hypertensive rats and angiotensin II-exposed microglial cells: Role of renin-angiotensin system. Redox Biol 26: 101295, 2019.

18. Chen L, Yang R, Qiao W, Zhang W, Chen J, Mao L, Goltzman D and Miao D: 1,25-Dihydroxyvitamin D exerts an antiaging role by activation of Nrf2-antioxidant signaling and inactivation of p16/p53-senescence signaling. Aging Cell 18: e12951, 2019.

19. Qin Q, Liu H, Shou J, Jiang Y, Yu H and Wang X: The inhibitor effect of RKIP on inflammasome activation and inflammasome-dependent diseases. Cell Mol Immunol 18: 992-1004, 2021.

20. Sharma BR and Kanneganti TD: NLRP3 inflammasome in cancer and metabolic diseases. Nat Immunol 22: 550-559, 2021.

21. Zhang X, Hu C, Kong CY, Song P, Wu HM, Xu SC, Yuan YP, Deng W, Ma ZG and Tang QZ: FNDC5 alleviates oxidative stress and cardiomyocyte apoptosis in doxorubicin-induced cardiotoxicity via activating AKT. Cell Death Differ 27: 540-555, 2020.

22. Nolfi-Donegan D, Braganza A and Shiva S: Mitochondrial electron transport chain: Oxidative phosphorylation, oxidant production, and methods of measurement. Redox Biol 37: 101674, 2020.

23. Byrne NJ, Rajasekaran NS, Abel ED and Bugger H: Therapeutic potential of targeting oxidative stress in diabetic cardiomyopathy. Free Radic Biol Med 169: 317-342, 2021.

24. Yang R, Zhang J, Li J, Qin R, Chen J, Wang R, Goltzman D and Miao D: Inhibition of Nrf2 degradation alleviates age-related osteoporosis induced by 1,25-Dihydroxyvitamin D deficiency. Free Radic Biol Med 178: 246-261, 2022.

25. Bosworth CR, Levin G, Robinson-Cohen C, Hoofnagle AN, Ruzinski J, Young B, Schwartz SM, Himmelfarb J, Kestenbaum B and de Boer IH: The serum 24,25-dihydroxyvitamin D concentration, a marker of vitamin D catabolism, is reduced in chronic kidney disease. Kidney Int 82: 693-700, 2012.

26. Zhang W, Chen L, Zhang L, Xiao M, Ding J, Goltzman D and Miao D: Administration of exogenous 1,25(OH)2D3 normalizes overactivation of the central renin-angiotensin system in 1alpha (OH)ase knockout mice. Neurosci Lett 588: 184-189, 2015.

27. Yang R, Chen J, Zhang J, Qin R, Wang R, Qiu Y, Mao Z, Goltzman D and Miao D: 1,25-Dihydroxyvitamin D protects against age-related osteoporosis by a novel VDR-Ezh2-p16 signal axis. Aging Cell 19: e13095, 2020.

28. Tomczyk MM, Cheung KG, Xiang B, Tamanna N, Fonseca TA, Agarwal P, Kereliuk SM, Spicer V, Lin L, Treberg J, *et al*: Mitochondrial sirtuin-3 (SIRT3) prevents doxorubicin-induced dilated cardiomyopathy by modulating protein acetylation and oxidative stress. Circ Heart Fail 15: e8547, 2022.

29. Gu X, Gu B, Lv X, Yu Z, Wang R, Zhou X, Qiao W, Mao Z, Zuo G, Li Q, *et al*: 1, 25-dihydroxy-vitamin D3 with tumor necrosis factor-alpha protects against rheumatoid arthritis by promoting p53 acetylation-mediated apoptosis via Sirt1 in synoviocytes. Cell Death Dis 7: e2423, 2016.

30. Schindelin J, Arganda-Carreras I, Frise E, Kaynig V, Longair M, Pietzsch T, Preibisch S, Rueden C, Saalfeld S, Schmid B, *et al*: Fiji: An open-source platform for biological-image analysis. Nat Methods 9: 676-682, 2012.

31. Livak KJ and Schmittgen TD: Analysis of relative gene expression data using real-time quantitative RCR and the 2(-Delta Delta C(T)) method. Methods 25: 402-408, 2001.

32. Chen B and Zhang JP: Bcl-xL is required for the protective effects of low-dose berberine against doxorubicin-induced cardiotoxicity through blocking apoptosis and activating mitophagy-mediated ROS elimination. Phytomedicine 101: 154130, 2022.

33. Bi Y, Xu H, Wang X, Zhu H, Ge J, Ren J and Zhang Y: FUNDC1 protects against doxorubicin-induced cardiomyocyte PANoptosis through stabilizing mtDNA via interaction with TUFM. Cell Death Dis 13: 1020, 2022.

34. Shi S, Chen Y, Luo Z, Nie G and Dai Y: Role of oxidative stress and inflammation-related signaling pathways in doxorubicin-induced cardiomyopathy. Cell Commun Signal 21: 61, 2023.

35. Coll RC, Schroder K and Pelegrin P: NLRP3 and pyroptosis blockers for treating inflammatory diseases. Trends Pharmacol Sci 43: 653-668, 2022.

36. Harris J and Borg NA: The multifaceted roles of NLRP3-modulating proteins in virus infection. Front Immunol 13: 987453, 2022.

37. Moena D, Nardocci G, Acevedo E, Lian J, Stein G, Stein J and Montecino M: Ezh2-dependent H3K27me3 modification dynamically regulates vitamin D3-dependent epigenetic control of CYP24A1 gene expression in osteoblastic cells. J Cell Physiol 235: 5404-5412, 2020.

38. Park S, Kim GW, Kwon SH and Lee JS: Broad domains of histone H3 lysine 4 trimethylation in transcriptional regulation and disease. FEBS J 287: 2891-2902, 2020.

39. Kang SJ and Chun T: Structural heterogeneity of the mammalian polycomb repressor complex in immune regulation. Exp Mol Med 52: 1004-1015, 2020.

40. Rawat PS, Jaiswal A, Khurana A, Bhatti JS and Navik U: Doxorubicin-induced cardiotoxicity: An update on the molecular mechanism and novel therapeutic strategies for effective management. Biomed Pharmacother 139: 111708, 2021.

41. Wang Y, Zhu J and DeLuca HF: Where is the vitamin D receptor? Arch Biochem Biophys 523: 123-133, 2012.

42. Chen L, Yang R, Qiao W, Yuan X, Wang S, Goltzman D and Miao D: 1,25-Dihydroxy vitamin D prevents tumorigenesis by inhibiting oxidative stress and inducing tumor cellular senescence in mice. Int J Cancer 143: 368-382, 2018.

43. Spasovski G: Advances in pharmacotherapy for hyperphosphatemia in renal disease. Expert Opin Pharmacother 16: 2589-2599, 2015.

44. Sutterwala FS, Haasken S and Cassel SL: Mechanism of NLRP3 inflammasome activation. Ann N Y Acad Sci 1319: 82-95, 2014.

45. Cao R, Ma Y, Li S, Shen D, Yang S, Wang X, Cao Y, Wang Z, Wei Y, Li S, *et al*: 1,25(OH)(2) D(3) alleviates DSS-induced ulcerative colitis via inhibiting NLRP3 inflammasome activation. J Leukoc Biol 108: 283-295, 2020.

46. Tulk SE, Liao KC, Muruve DA, Li Y, Beck PL and MacDonald JA: Vitamin D(3) metabolites enhance the NLRP3-dependent secretion of IL-1β from human THP-1 monocytic cells. J Cell Biochem 116: 711-720, 2015.

47. Poli G, Fabi C, Bellet MM, Costantini C, Nunziangeli L, Romani L and Brancorsini S: Epigenetic mechanisms of inflammasome regulation. Int J Mol Sci 21: 5758, 2020.

48. Dai X, Liao R, Liu C, Liu S, Huang H, Liu J, Jin T, Guo H, Zheng Z, Xia M, et al: Epigenetic regulation of TXNIP-mediated oxidative stress and NLRP3 inflammasome activation contributes to SAHH inhibition-aggravated diabetic nephropathy. Redox Biol 45: 102033, 2021.
49. Lecoeur H, Prina E, Rosazza T, Kokou K, N'Diaye P, Aulner N, Varet H, Bussotti G, Xing Y, Milon G, et al: Targeting macrophage histone H3 modification as a leishmania strategy to dampen the NF-kappaB/NLRP3-mediated inflammatory response. Cell Rep 30: 1870-1882, 2020.
50. Lecoeur H, Rosazza T, Kokou K, Varet H, Coppee JY, Lari A, Commere PH, Weil R, Meng G, Milon G, et al: Leishmania amazonensis subverts the transcription factor landscape in dendritic cells to avoid inflammasome activation and stall maturation. Front Immunol 11: 1098, 2020.
51. Uckelmann M and Sixma TK: Histone ubiquitination in the DNA damage response. DNA Repair (Amst) 56: 92-101, 2017.
52. Chan HL and Morey L: Emerging roles for polycomb-group proteins in stem cells and cancer. Trends Biochem Sci 44: 688-700, 2019.
53. Barbour H, Daou S, Hendzel M and Affar EB: Polycomb group-mediated histone H2A monoubiquitination in epigenome regulation and nuclear processes. Nat Commun 11: 5947, 2020.
54. Han X, Zhu N, Wang Y and Cheng G: 1,25(OH)2D3 inhibits osteogenic differentiation through activating beta-catenin signaling via downregulating bone morphogenetic protein 2. Mol Med Rep 22: 5023-5032, 2020.